

Dark matter freeze-in via a light fermion mediator: forbidden decay and scattering

Shao-Ping Li^a

^a*Institute of High Energy Physics, Chinese Academy of Sciences, Beijing 100049, China*

E-mail: spli@ihep.ac.cn

ABSTRACT: The connection between a hidden nonthermal sector and a thermal plasma can be established by a light thermal fermion mediator. When the fermion mediator is much lighter than the hidden species, kinematically forbidden decay of the mediator can be opened at finite temperatures to produce the hidden species. Unlike bosons having quartic couplings, renormalizable forbidden fermion decay generically shares the same order of couplings with the scattering. We present a dedicated investigation into the freeze-in dark matter production via a thermal fermion mediator. We demonstrate that the plasma-induced decay rate differs from that calculated via the tree-level amplitude, but the former can be obtained from the latter via constant rescaling. Furthermore, we find that the relative effect of the forbidden decay and the scattering on the dark matter relic density can be simply estimated via the thermal coupling between the plasma and the mediator. Applying to different thermal interactions, we show that the forbidden decay contribution can reach the level of 4%–45% for a thermal coupling at 0.1–1.

Contents

1	Introduction	1
2	The Yukawa portals	3
3	Forbidden decay	5
3.1	Boltzmann equation	5
3.2	Spectral density of the fermion mediator	7
3.3	Collision rate	10
3.3.1	One-loop retarded amplitude	10
3.3.2	Tree-level amplitude	11
4	Scattering	13
4.1	Double counting and resonant enhancement	13
4.2	Tree-level scattering amplitude without thermal correction	14
5	DM relic density	16
6	Application to different thermal Yukawa interactions	19
6.1	Right-handed fermion mediator	19
6.2	Left-handed fermion mediator	21
7	Conclusions	22
A	Thermal one-loop amplitudes	23
A.1	The DM part	23
A.2	The fermion mediator part	23

1 Introduction

A hidden nonthermal species can be created in the early universe from the thermal plasma via a light mediator [1]. If the hidden sector consists of feebly interacting dark matter (DM), the direct DM detection could be challenging. However, a light mediator connecting the DM with the standard model (SM) can provide a striking avenue to test the feeble DM scenarios if the connection between the mediator and the SM is relatively strong and/or the mediator is relatively light [2].

DM production via mediators have received great interests over the past years. For instance, the millicharged DM production from a vector mediator [3–6] and the sterile neutrino DM production via a scalar mediator [7–11]. There are also interesting DM

scenarios via a fermion mediator. A typical example is that the sterile neutrino itself can be the mediator to connect a stable dark sector with the SM particles [12–22].

The phenomenology of DM production via mediators is fruitful. The annihilation from DM to the mediator could generate secondary fluxes consisting of SM particles via subsequent mediator decay [23, 24]. If the mediator is sufficiently light, it can contribute to the energy density of the early universe, thereby leaving imprints in the epochs detectable by the big bang nucleosynthesis and the cosmic microwave background [25]. Furthermore, if the mediator is long-lived, it can generate displaced vertices and could be detected at the LHC [26–29].

Generally, if the mediator particle is heavier than the dark sector in vacuum, the mediator decay to DM plays the dominant role in generating the DM relic density, unless there is sufficient mass mixing between the mediator and the DM [30]. If the mediator is much lighter than the dark sector, the decay channel is kinematically forbidden in vacuum and the scattering/annihilation would be naturally considered as the dominant production channel. In this latter case, however, if the mediator has a strong connection with the thermal particles, the mediator will acquire non-negligible corrections from the plasma and such thermal corrections can open up DM production channels which are kinematically forbidden in vacuum.

Forbidden channels in generating the observed DM relic density were considered in the thermal freeze-out paradigm [31, 32], where the relic density is determined by the DM annihilation channel forbidden in vacuum. In the freeze-in paradigm [7, 8, 33–35], forbidden decay was considered in Refs. [5, 36–38] for a vector mediator and in Refs. [11, 39–41] for a scalar mediator. For a fermion mediator, on the other hand, the mediator heavier than the DM is usually considered so that the forbidden decay contributes only as a subdominant or negligible correction to the vacuum decay (see e.g. [13, 16, 21]), while few attention is drawn to the light mass regime where forbidden decay and scattering could coexist to generate the relic density. Filling in this gap underlies the purpose of this work.

A thermal fermion mediator differs by several aspects from a boson mediator. Since the boson can have a renormalizable self-interaction, such as the gluons and an SM scalar singlet, the forbidden decay rate can carry lower-order couplings with respect to the scattering so that the former becomes the dominant production channel [37, 39, 40], unless the quartic interactions are suppressed with respect to Yukawa or trilinear-boson interaction [41]. For fermion mediators, renormalizable interactions imply that there is no tree-level quartic fermion interaction, and the forbidden fermion decay rate would generically carry the same order of couplings with respect to the scattering, as will shown in this work. Given that the rates from the forbidden decay and the scattering have the same order of couplings, it becomes less clear to see the relative effect of the forbidden decay and the associated scattering on the DM relic density and hence worth examining in detail the interplay between the two channels.

On the other hand, the modified dispersion relation of a scalar at finite temperatures retains the vacuum form in the Hard-Thermal-Loop (HTL) approximation [42–46], which allows the calculation of forbidden scalar decay to follow a tree-level amplitude [11, 41]. For fermion mediators, however, the modified dispersion relation is more involved due to

the helicity structure [47–49]. It then becomes nontrivial to see if and how the forbidden decay can be simply obtained via a tree-level amplitude, where the thermal fermion mass is put in by hand. Such an issue was considered in leptogenesis [50] and in this paper, we bring it for the first time to the freeze-in DM production and provide a comprehensive analysis on the difference between the tree-level and one-loop results.

This work is concerned with a dedicated analysis of freeze-in DM production via a light thermal fermion mediator which cannot decay to DM at zero temperature. We will concentrate on the computation of the DM relic density from the forbidden fermion decay and the scattering. We will calculate the forbidden decay rates from a thermal one-loop amplitude and a vacuum tree-level amplitude, respectively, and find that the former can be simply obtained from the latter with some constant rescaling. The comparison between the forbidden decay and the scattering shows a rather simple dependence on the thermal coupling constant, which enables us to include the plasma-induced decay in the scattering channel efficiently. This work complements the studies of nonthermal DM production through a light fermion mediator and provides a simple and comprehensive method to treat the forbidden decay for a wide range of fermion mediator scenarios. In particular, the results shown here can help us to gain a clear insight into the importance of forbidden fermion decay.

The remainder of this paper is outlined as follows. In Sec. 2, we present a simplified but general scenario to illustrate the freeze-in DM production via a light thermal fermion mediator. Within the simplified scenario, we calculate the forbidden decay rate in Sec. 3 and make a comparison with the rate derived from the vacuum tree-level amplitude. In Sec. 4, we first point out some subtleties concerning the double-counting issue and the s -channel resonant enhancement, and then evaluate the scattering rate without thermal corrections. In Sec. 5, we determine the DM relic density from the forbidden decay and scattering channels respectively. We then apply the relation between the two channels to some specific thermal interactions in Sec. 6. Conclusions are made in Sec. 7 and some technical details are relegated to the appendix.

2 The Yukawa portals

We first consider a simplified scenario in which the nonthermal dark sector consists of a Dirac fermion χ and a scalar ϕ . The connection between the dark sector and a Dirac fermion mediator ψ is realized by the following Yukawa interaction:

$$\mathcal{L}_{\text{DM}} = y_\chi \bar{\psi}_R \chi_L \phi + \text{h.c.} \quad (2.1)$$

To ensure a thermal history of ψ , we consider a typical Yukawa interaction between the mediator and the thermal plasma, i.e.,

$$\mathcal{L}_\psi = y_\psi \bar{\psi}_R \eta_L \varphi + \text{h.c.}, \quad (2.2)$$

where both the fermion η and the scalar φ live in the thermal plasma. For clarity, we assume that the fermion mediator is right-handed in (2.1), but it should be mentioned that

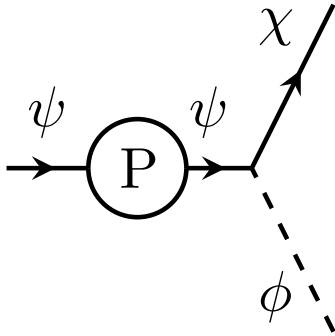


Figure 1. Forbidden fermion decay due to the thermal contact with the plasma (P).

a left-handed fermion mediator is also possible. In Sec. 6, we shall discuss some specific models for both right- and left-handed fermion mediators.

Note that the fermion mediator can also have gauge interactions, e.g.,

$$V_\mu \bar{\psi}_R \gamma^\mu \psi_R, \quad (2.3)$$

with V_μ a $U(1)$ gauge boson. Nevertheless, when the mediator is thermalized via the gauge interaction, gauge invariance requires that either χ or ϕ should be also charged under the gauge $U(1)$ symmetry. In this case, either χ or ϕ will reach thermal equilibrium in the early universe, which can lead to significant difference from the situation where both χ and ϕ are far from equilibrium. For instance, when ϕ is in thermal equilibrium, the decay $\phi \rightarrow \chi + \psi$ and the scattering $\phi + \psi \rightarrow \chi + V_\mu$ can dominate the production of χ , both of which are suppressed instead when ϕ is far from equilibrium. Besides, the Landau-Pomeranchuk-Migdal effect induced by soft vector boson exchange would also be of leading-order contribution [51] and should be taken into account consistently. Throughout this work, we will consider for simplicity a dark sector consisting of nonthermal χ and ϕ , leaving a thermal χ or ϕ for future studies.

We will consider the situation where all the relevant thermal particles, i.e., ψ , η , and φ have vacuum masses much lighter than the dark sector, which is readily applicable to super-heavy DM [52, 53]. In this light mass regime, the freeze-in temperature of the DM is determined by the highest scale in the dark sector. Besides, without a mild mass difference between the initial and final states, as implemented in forbidden annihilation channels [31, 32], the nonrelativistic annihilation of ψ , η , and φ to the dark sector is essentially disallowed. Consequently, the DM relic density would basically be independent of the vacuum masses of the thermal particles. In the following discussions, we assume $m_\chi < m_\phi$ for clarity. In this mass regime, either χ can be the only DM candidate or both χ and ϕ contribute to the observed DM relic density, though the later case is ruled out if $m_\phi \gg 1$ GeV.

Before going into the detailed calculation, let us take a diagrammatic view of the relation between the forbidden fermion decay and the scattering. In Fig. 1, the fermion ψ receives a thermal mass correction from the self-energy diagram, where P denotes the

plasma. Such a correction opens the kinematic space so that the decay $\psi \rightarrow \chi + \phi$ becomes possible at finite temperatures. Dimensional analysis implies that the squared amplitude scales as $y_\chi^2 m_\psi^2$ at sufficiently high temperatures, where m_ψ denotes the thermal mass. The interaction given in (2.2) implies that $m_\psi^2 \sim y_\psi^2 T^2$. Therefore, the forbidden decay rate at high temperatures scales as

$$\gamma_{\text{decay}} \sim y_\chi^2 y_\psi^2 T^4. \quad (2.4)$$

The thermal self-energy amplitude in general has an imaginary part, which corresponds to on-shell thermal particles running in the loop. In this case, Fig. 1 also presents a scattering channel $\eta + \varphi \rightarrow \psi \rightarrow \chi + \phi$. It is easy to see that the squared amplitude of the scattering also depends on y_χ and y_ψ quadratically, and the scattering rate at high temperatures would scale as

$$\gamma_{\text{scat}} \sim y_\chi^2 y_\psi^2 T^4 \sim \gamma_{\text{decay}}. \quad (2.5)$$

It should be mentioned that the self-energy correction for relativistic fermions generically predicts a thermal mass with a form $\sim yT$, where y is the dimensionless coupling between the fermion mediator and the plasma¹. Such a fermion mediator in renormalizable interactions differs from a vector/scalar boson mediator which has a strong quartic self-coupling λ . The leading-order thermal mass for such bosons scales as $\sim \sqrt{\lambda}T$ and the resulting forbidden boson decay has a rate $\gamma_{\text{decay}} \propto \lambda T^4$ while the associated scattering rate gives $\gamma_{\text{scat}} \propto \lambda^2 T^4$. In such situations, the forbidden decay can dominate the DM production, as considered in Refs. [37, 39, 40].

Therefore, unlike the forbidden boson decay, the scattering is present at the same order of couplings whenever forbidden fermion decay is opened in renormalizable interactions, and vice versa. They coexist to produce the DM at finite temperatures. We will show in the subsequent content that there is a close relation between the two channels, which allows us to see the relative effect on the DM production in a simple way.

3 Forbidden decay

3.1 Boltzmann equation

The decay process $\psi \rightarrow \chi + \phi$ is kinematically forbidden in vacuum but opened at finite temperatures. The forbidden decay rate that determines the density evolution in the dark sector can be calculated in the finite-temperature field theory [46]. Concerning the production of χ , the Boltzmann equation can be written as

$$\frac{dn_\chi}{dt} + 3Hn_\chi = \int \frac{d^3p_\chi}{(2\pi)^3} (f_\chi^{\text{eq}} - f_\chi) \Gamma_\chi, \quad (3.1)$$

¹We are concerned with IR-dependent freeze-in so that the production of DM comes from renormalizable interactions. The conclusions drawn in this paper are hence responsible for renormalizable interactions. For non-renormalizable interactions, the freeze-in production of DM is not IR but UV dependent [54].

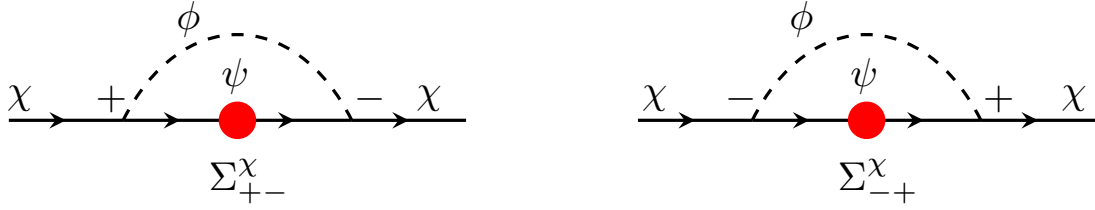


Figure 2. The one-loop self-energy diagrams of χ that contribute to the imaginary part of the retarded amplitude $\text{Im}\Sigma_R^\chi$ in the forbidden decay. Here \pm in the vertices denote the thermal indices in the doubled space of real-time formalism and the red blob denotes the resummed ψ propagator at finite temperatures.

where $f_\chi^{\text{eq}}(E_\chi) = (e^{E_\chi/T} + 1)^{-1}$ is the Fermi-Dirac distribution function of χ and $H \approx 1.66\sqrt{g_\rho}T^2/M_{\text{Pl}}$ is the Hubble parameter with the effective number of relativistic degrees of freedom g_ρ for energy density and the Planck mass $M_{\text{Pl}} \approx 1.22 \times 10^{19}$ GeV.

The production rate Γ_χ at finite temperatures is related to the one-loop retarded self-energy of χ via [55]

$$\Gamma_\chi(P) = -g_\chi \frac{\text{Tr}[(\not{P} + m_\chi)\text{Im}\Sigma_R^\chi(P)]}{2E_p}, \quad (3.2)$$

with $P_\mu = (E_p, \vec{p})$ the 4-momentum of χ and $\text{Im}\Sigma_R^\chi$ the imaginary part of the one-loop retarded amplitude. It should be mentioned that the factor of 2 in the denominator of Eq. (3.2) results from the spin sum and average over the Dirac spinor χ . Therefore, the collision rate in the Boltzmann Eq. (3.1) should be further multiplied by the spin degrees of freedom $g_\chi = 2$ [56] so as to obtain a collision term without spin average. For a nonthermal DM in the freeze-in paradigm, we expect $f_\chi \ll f_\chi^{\text{eq}}$ so that f_χ can be neglected in the determination of the DM relic density. In the end, the relic density should be multiplied by a factor of 2 to take into account the antiparticle ($\bar{\chi}$) contribution.

In the real-time formalism, the imaginary part of the retarded amplitude Σ_R^χ can be computed from the one-loop self-energy diagrams shown in Fig. 2, with

$$\text{Im}\Sigma_R^\chi(P) = \frac{i}{2} [\Sigma_{+-}^\chi(P) - \Sigma_{-+}^\chi(P)]. \quad (3.3)$$

Using the expressions of $\Sigma_{+-}^\chi, \Sigma_{-+}^\chi$ from Appendix A.1, we obtain

$$\text{Im}\Sigma_R^\chi(P) = \frac{y_\chi^2}{2(2\pi)^2} \int d^4K \text{sign}(k_0 - p_0) f_\psi(k_0) \delta[(K - P)^2 - m_\phi^2] \rho_\psi(K), \quad (3.4)$$

where $\text{sign}(k_0 - p_0)$ denotes the sign function and $f_\psi(k_0) = (e^{k_0/T} + 1)^{-1}$. In the above equation, we have neglected the scalar distribution function f_ϕ since ϕ is sparse during the freeze-in production. $\rho_\psi(K)$ is the spectral density that encapsulates the thermal corrections to ψ , as we shall derive below.

3.2 Spectral density of the fermion mediator

The spectral density is defined via the resummed ψ propagators,

$$S_{+-} = -f_\psi(\tilde{G}_R - \tilde{G}_A) \equiv -2\pi i f_\psi(k_0)\rho_\psi(K), \quad (3.5)$$

$$S_{-+} = [1 - f_\psi(k_0)](\tilde{G}_R - \tilde{G}_A) \equiv 2\pi i [1 - f_\psi(k_0)]\rho_\psi(K), \quad (3.6)$$

where \tilde{G}_R/\tilde{G}_A are the resummed retarded/advanced propagators. Since the spectral density defined above encapsulates the thermal corrections in the form of $\tilde{G}_R - \tilde{G}_A$, we should first be aware of how the thermal corrections appear in the resummed retarded and advanced propagators.

In general, the retarded amplitude for fermion self-energy can be parameterized as² [47]

$$-\Sigma_R^\psi(K) \equiv (a_L P_L + a_R P_R)\not{K} + (b_L P_L + b_R P_R)\not{U}, \quad (3.7)$$

where $P_{L,R}$ are the chirality projection operators and U_μ is the four-velocity of the plasma with $U_\mu U^\mu = 1$. In the rest frame, $U_\mu = (1, 0, 0, 0)$. Since the parity of the fermion mediator from the interactions given in Sec. 2 is explicitly broken, and at sufficiently high temperatures ψ is effectively massless³, we are essentially working in a chirality-symmetric and parity-broken theory, where a_L, b_L are nonzero while $a_R, b_R = 0$. The coefficients a_L, b_L can be calculated by left-multiplying $\Sigma_R^\psi(K)$ with \not{K} and \not{U} , and then evaluating the trace. The general expressions read:

$$a_L = \frac{1}{2k^2} \left(\text{Tr}[\not{K}\Sigma_R^\psi(K)] - k_0 \text{Tr}[\not{U}\Sigma_R^\psi(K)] \right), \quad (3.8)$$

$$b_L = -\frac{1}{2k^2} \left(k_0 \text{Tr}[\not{K}\Sigma_R^\psi(K)] - K^2 \text{Tr}[\not{U}\Sigma_R^\psi(K)] \right), \quad (3.9)$$

with $K^2 = k_0^2 - k^2$.

Given Eq. (3.7), the resummed retarded propagator in the chirality-symmetric and parity-broken regime can be written as

$$\tilde{G}_R = P_R \frac{(1 + a_L)\not{K} + b_L\not{U}}{[(1 + a_L)k_0 + b_L]^2 - [(1 + a_L)k]^2 + i\text{sign}(k_0)\epsilon} P_L, \quad (3.10)$$

and the advanced propagator can be similarly obtained by using $\Sigma_A^\psi = \Sigma_R^{\psi*}$. The difference $\tilde{G}_R - \tilde{G}_A$ can be conveniently written in terms of the helicity eigenstates [48, 49],

$$\tilde{G}_R - \tilde{G}_A = \sum_{\pm} \frac{-2i(\text{Im}\Delta_{\pm} \mp \text{sign}(k_0)\epsilon)}{[\text{Re}\Delta_{\pm}]^2 + [\text{Im}\Delta_{\pm} + \epsilon]^2} \hat{P}_{\pm}, \quad (3.11)$$

²The minus sign is defined for convenience, which results in $1 + a$ in the denominator of propagators.

³If ψ acquires its vacuum mass via the Higgs or Higgs-like mechanism, then ψ is exactly massless above the cross-over or phase-transition temperature.

where $\Delta_{\pm}(K) \equiv (1 + a_L)k_0 + b_L \pm (1 + a_L)k$, and the helicity operators are defined by

$$\hat{P}_{\pm} \equiv P_R \frac{\gamma^0 \pm \vec{e}_k \cdot \vec{\gamma}}{2} P_L, \quad (3.12)$$

with $\vec{e}_k \equiv \vec{k}/k$.

The spectral density ρ_{ψ} can be decomposed into the on-shell and off-shell parts,

$$\rho_{\psi}(K) \equiv \rho_{\psi,\text{on}}(K) + \rho_{\psi,\text{off}}(K). \quad (3.13)$$

The kinematically forbidden decay stems from the on-shell part $\rho_{\psi,\text{on}}(K)$, as will be derived in this section, while the off-shell part $\rho_{\psi,\text{off}}(K)$ arises from nonzero $\text{Im}\Delta_{\pm}$ and corresponds to the scattering channels. Note that the on-shell propagation of the fermion mediator could also result from the scattering channel. To avoid potential double counting, $\rho_{\psi,\text{on}}(K)$ defined above corresponds to $\text{Im}\Delta_{\pm} = 0$. Then, from Eq. (3.11) the on-shell part is given by

$$\rho_{\psi,\text{on}}(K) = \sum_{\pm} \pm \text{sign}(k_0) \left| \frac{\partial \text{Re}\Delta_{\pm}}{\partial k_0} \right|^{-1} \left[\delta(k_0 - \omega_1^{\pm}) + \delta(k_0 - \omega_2^{\pm}) \right] \hat{P}_{\pm}. \quad (3.14)$$

In general, there are two solutions $\omega_{1,2}$ to $\text{Re}\Delta_i = 0$ for each helicity operator \hat{P}_i . In the free limit, $a_L = b_L = 0$ and $\Delta_{\pm} = k_0 \pm k$. It can be verified that S_{+-}, S_{-+} given in Eqs. (3.5) and (3.6) reduce to the known forms [46]:

$$S_{+-}(K) = 2\pi i \text{sign}(k_0) f_{\psi}(k_0) \delta(K^2) \not{K}, \quad (3.15)$$

$$S_{-+}(K) = -2\pi i \text{sign}(k_0) [1 - f_{\psi}(k_0)] \delta(K^2) \not{K}. \quad (3.16)$$

To proceed with Eq. (3.4), the remaining task is to evaluate the real part of the resummed amplitude Σ_R^{ψ} , which depends on the thermal interaction specified in Sec. 2.

The one-loop retarded self-energy diagram of ψ from (2.2) is similar to Fig. 2, with the resummed fermion propagators replaced by the free ones given in Eqs. (3.15) and (3.16). The inclusion of resummed propagators for thermal η, φ in Fig. 2 is of higher order under the perturbative HTL technique. Substituting Eqs. (A.7) and (A.8) into Eqs. (3.8) and (3.9), we obtain the real part of the coefficients a_L, b_L as

$$\text{Re}a_L = \frac{m_{\psi}^2(T)}{k^2} \left(1 + \frac{k_0}{2k} \ln \left| \frac{k_0 - k}{k_0 + k} \right| \right), \quad (3.17)$$

$$\text{Re}b_L = -\frac{m_{\psi}^2(T)}{k} \left(\frac{k_0}{k} - \frac{1}{2} \left(1 - \frac{k_0^2}{k^2} \right) \ln \left| \frac{k_0 - k}{k_0 + k} \right| \right), \quad (3.18)$$

where the thermal mass is defined by

$$m_{\psi}^2(T) = \frac{y_{\psi}^2}{16} T^2 \equiv \kappa^2 T^2, \quad (3.19)$$

where κ is defined as a thermal parameter quantifying the amount of thermal corrections.

The results given in Eqs. (3.17) and (3.18) are consistent with Ref. [47] except that the logarithmic function is expressed by the modulus of momentum. The modulus arises when we integrate $\cos\theta$ in Eq. (A.8) without restricting ourselves to the timelike regime $K^2 = k_0^2 - k^2 > 0$. Nevertheless, we will see below that an on-shell fermion with Eqs. (3.17) and (3.18) cannot propagate in the spacelike region. The modified dispersion relation is given by

$$[(1 + \text{Re}a_L)k_0 + \text{Re}b_L]^2 - [(1 + \text{Re}a_L)k]^2 = 0. \quad (3.20)$$

For a weak-coupling theory $y_\psi \lesssim 1$, we expect $\text{Re}a_L < 1$. Neglecting the higher-order terms $\text{Re}a_L^2$ and $\text{Re}b_L^2$, we obtain the approximate dispersion relation:

$$k_0^2 - k^2 \approx -\frac{2k_0\text{Re}b_L}{1 + 2\text{Re}a_L}. \quad (3.21)$$

Then given Eqs. (3.17) and (3.18), it is straightforward to verify that there is no solution to the above equation for $k_0^2 - k^2 < 0$. Therefore, the absolute symbol in Eqs. (3.17) and (3.18) should be removed.

The thermal mass defined in Eq. (3.19) is proportional to the quadratic Casimir invariant of the fermion mediator representation in gauge interactions, as well as the gauge degeneracy of the loop particles in Yukawa interactions [47]. For the freeze-in DM production considered here, the fermion mediator should be a SM singlet so there is no gauge contribution to the thermal mass. However, the loop particles could be gauge multiplets. For instance, if the scalar φ and the fermion η are gauge $SU(2)_L$ doublets, then an additional factor of 2 arises in $m_\psi^2(T)$. This is readily seen by the fact that there are two gauge components in the loop. On the other hand, if φ and η are gauge $SU(3)_c$ triplets, a factor of 3 due to the color degrees of freedom arises in $m_\psi^2(T)$.

It should also be mentioned that the results given in Eqs. (3.17)-(3.19) (see also the appendix) are obtained in the HTL approximation which keeps the leading-order coupling (y_ψ) contributions. Under the perturbative region $y_\psi < \sqrt{4\pi}$, there is no definite upper limit of the coupling for the HTL validity. It was pointed out in Ref. [57] that a coupling at ~ 1 can still give qualitatively correct result under the HTL approximation. In general, larger couplings lead to a poorer accuracy under the HTL approximation. Therefore, we will impose $y_\psi < 1$ as a conservative upper limit for the Yukawa interaction when applying the HTL approximation. In particular, we will consider a weak-coupling regime where

$$0.1 < y_\psi < 1, \quad (3.22)$$

in subsequent discussions.

In the following analyses, we will take κ as a free thermal parameter. It is noteworthy that the upper bound of κ from the condition in Eq. (3.22) depends on the specific thermalization interaction between the mediator and the plasma, as well as the flavor effects from Yukawa interactions. For instance, if the fermion mediator couples comparably to three

SM quark doublets via a leptoquark doublet, the upper bound of κ is given by $\kappa < 1.1$. In Sec. 6, we will consider some specific examples and present the corresponding limit of κ and its impact on forbidden decay contribution.

3.3 Collision rate

3.3.1 One-loop retarded amplitude

Given the expressions of $\text{Re}a_L$, $\text{Re}b_L$ in Eqs. (3.17) and (3.18), the on-shell spectral density from Eq. (3.14) can be simplified as

$$\rho_{\psi,\text{on}}(K) = \sum_{\pm} \pm \frac{k_0^2 - k^2}{2m_\psi^2(T)} \text{sign}(k_0) [\delta(k_0 \mp \omega_1) + \delta(k_0 \pm \omega_2)] \hat{P}_{\pm}, \quad (3.23)$$

where $\omega_{1,2}$ are the solutions to the modified dispersion relation (3.20) and can be analytically expressed in terms of the Lambert W-function [50]:

$$\omega_1 = -k \frac{W_0(-e^{-2k^2/m_\psi^2-1}) - 1}{W_0(-e^{-2k^2/m_\psi^2-1}) + 1}, \quad \omega_2 = k \frac{W_{-1}(-e^{-2k^2/m_\psi^2-1}) - 1}{W_{-1}(-e^{-2k^2/m_\psi^2-1}) + 1}, \quad (3.24)$$

with $\omega_{1,2} > k$.

Substituting Eqs. (3.4) and (3.2) into the collision term in Eq. (3.1), we arrive at the decay rate

$$C_{\chi,\text{dec}} = \frac{y_\chi^2}{32\pi^3 m_\psi^2(T)} \int_{m_\chi}^{\infty} dp_0 f_\chi^{\text{eq}}(p_0) \times \int_0^{\infty} dk \sum_{i=1,2} \mp \Theta_i(\omega_i^2 - k^2) f_\psi(\omega_i) (\pm k^2 \mp \omega_i^2 + 2p_0(k \pm \omega_i) \mp \delta m^2), \quad (3.25)$$

where $\delta m^2 \equiv m_\chi^2 - m_\phi^2 < 0$ and the symbol Θ_i imposes a restriction on the momentum integration from Eq. (3.4). Integrating the angle via the Dirac $\delta[(K-P)^2 - m_\phi^2]$ in Eq. (3.4), we find that in the timelike region $K^2 > 0$ the restriction turns out to be

$$\frac{K^2 + \delta m^2}{2(k_0 + k)} < p_0 < \frac{K^2 + \delta m^2}{2(k_0 - k)}, \quad k_0 - p_0 > 0. \quad (3.26)$$

Therefore, Θ_i is given by the Heaviside θ -function with

$$\Theta_i = \theta [(2p_0 k)^2 - (\omega_i^2 - k^2 + \delta m^2 - 2p_0 \omega_i)^2]. \quad (3.27)$$

The solutions $\omega_{1,2}$ from the modified dispersion relation are shown in Fig. 3 for $k/T < 1$ and $k/T > 1$, respectively. It can be seen that when k becomes larger, the ω_1 -mode approaches a dispersion relation $\omega_1 \approx k$ while the ω_2 -mode approaches a vacuum-like dispersion relation with an asymptotic mass $\sqrt{2}m_\psi(T)$ [50, 58–60]. It allows us to compute

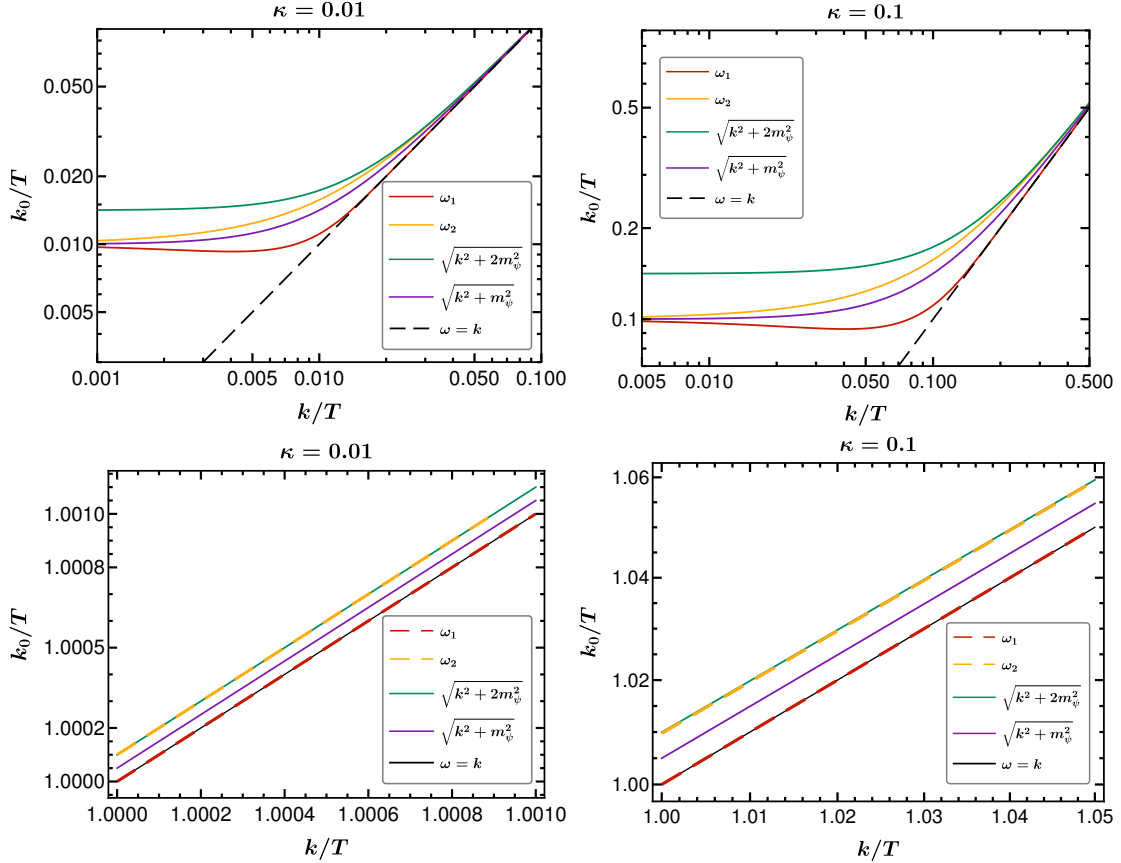


Figure 3. The behavior of dispersion relation (3.20) at $k/T < 1$ (top) and $k/T > 1$ (bottom), where the thermal parameter is set by $\kappa = 0.01, 0.1$, respectively.

Eq. (3.25) with the following approximations:

$$\omega_1^2 - k^2 \approx 0, \quad \omega_2^2 - k^2 \approx 2m_\psi^2(T). \quad (3.28)$$

Note that when the thermal coupling κ becomes smaller, the above approximations can already be accurate at lower momenta, as can be seen from the top of Fig. 3. With Eq. (3.28), the collision rate of the forbidden decay $C_{\chi,\text{dec}}$ reads

$$C_{\chi,\text{dec}} \approx \frac{y_\chi^2}{16\pi^3} \int_{m_\chi}^{\infty} dp_0 f_\chi^{\text{eq}}(p_0) \int_0^{\infty} dk \Theta_2 f_\psi(\omega_2) (2m_\psi^2(T) + 2p_0(k - \omega_2) + \delta m^2). \quad (3.29)$$

3.3.2 Tree-level amplitude

To see whether we can directly use the vacuum tree-level amplitude to compute the collision rate with the fermion thermal mass put in by hand, let us now calculate the relevant tree-level amplitude. As can be seen from Fig. 3, the ω_1 -mode quickly turns massless while the ω_2 -mode has an asymptotic mass $\sqrt{2}m_\psi(T)$ so that sufficient momentum space is opened in this mode for the forbidden decay. In the following, we will use the dispersion relation $\omega^2 - k^2 = 2m_\psi^2(T)$ to calculate the decay rate from the tree-level amplitude.

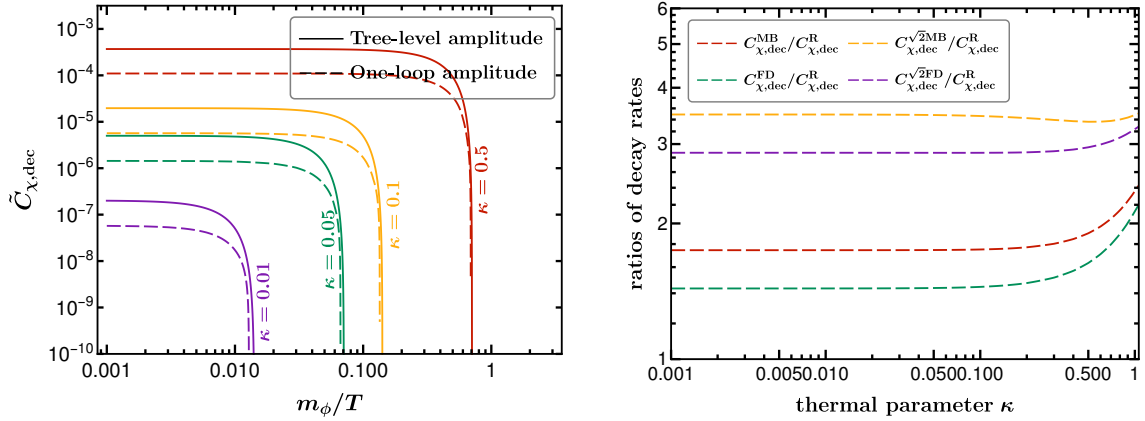


Figure 4. The comparison of forbidden decay rates from the one-loop retarded and vacuum tree-level amplitudes. Here $\tilde{C}_{\chi,\text{dec}} \equiv y_\chi^{-2} T^{-4} C_{\chi,\text{dec}}$. For $\kappa < 1$, the rates from the tree-level amplitude are overestimated by a factor of 1-4.

The squared amplitude of $\psi \rightarrow \chi + \phi$ is given by

$$\sum_s |\mathcal{M}|^2 \approx y_\chi^2 (2\kappa^2 T^2 - m_\phi^2), \quad (3.30)$$

where the approximation is obtained in the limit $m_\chi \ll m_\phi$. Note that the squared amplitude for the dispersion relation $\omega^2 - k^2 = m_\psi^2(T)$ can be simply obtained by replacing $\sqrt{2}\kappa$ with κ .

The collision rate is given by

$$\begin{aligned} C_{\chi,\text{dec}} &= \int \frac{d^3 p_\psi}{(2\pi)^3 2E_\psi} f_\psi^{\text{eq}} \int \frac{d^3 p_\chi}{(2\pi)^3 2E_\chi} \frac{d^3 p_\phi}{(2\pi)^3 2E_\phi} (2\pi)^4 \delta^4(P_\psi - P_\chi - P_\phi) \sum_s |\mathcal{M}|_{\psi \rightarrow \chi\phi}^2 \\ &\approx \frac{y_\chi^2 \kappa^3 K_1(\sqrt{2}\kappa)}{8\sqrt{2}\pi^3} \left(1 - \frac{m_\phi^2}{2\kappa^2 T^2}\right)^2 T^4, \end{aligned} \quad (3.31)$$

where K_1 is the modified Bessel function with $K_1(x) \approx 1/x$ for $x < 1$. In the last approximation we have used the Boltzmann distribution $f_\psi(E_\psi) = e^{-E_\psi/T}$ and kept the highest scale m_ϕ from the dark sector.

In the left panel of Fig. 4, we compare the decay rates obtained from Eq. (3.29) and Eq. (3.31) with different thermal parameter κ . Note that the rates from the two approaches share the same critical temperature

$$T_c \approx \frac{m_\phi}{\sqrt{2}\kappa}, \quad (3.32)$$

after which the decay is kinematically closed. We can see that the rate from the tree-level amplitude with an effective mass $\sqrt{2}m_\psi(T)$ is overestimated with respect to that from the one-loop retarded amplitude.

In the right panel of Fig. 4, we also show the ratios of various decay rates by evaluating

the vacuum tree-level amplitude with an effective mass $m_\psi(T)$ and taking the full Fermi-Dirac statistics for f_ψ^{eq} . Noticeably, a larger discrepancy between the retarded rate $C_{\chi,\text{dec}}^{\text{R}}$ and the vacuum one appears when the tree-level amplitude is evaluated with the asymptotic mass $\sqrt{2}m_\psi(T)$, as seen from the $C_{\chi,\text{dec}}^{\sqrt{2}\text{FD}}/C_{\chi,\text{dec}}^{\text{R}}$ and $C_{\chi,\text{dec}}^{\sqrt{2}\text{MB}}/C_{\chi,\text{dec}}^{\text{R}}$ curves. Instead, the vacuum rates with the dispersion relation $\omega^2 - k^2 = m_\psi^2(T)$ are more compatible with the retarded one. We found that for $\kappa < 0.2$ the ratios become constants and reach

$$\frac{C_{\chi,\text{dec}}^{\text{FD}}}{C_{\chi,\text{dec}}^{\text{R}}} \simeq 1.4, \quad \frac{C_{\chi,\text{dec}}^{\text{MB}}}{C_{\chi,\text{dec}}^{\text{R}}} \simeq 1.7, \quad (3.33)$$

in which $C_{\chi,\text{dec}}^{\text{FD}}$ and $C_{\chi,\text{dec}}^{\text{MB}}$ denote the vacuum rates with the Fermi-Dirac and Maxwell-Boltzman statistics, respectively, together with the dispersion relation $\omega^2 - k^2 = m_\psi^2(T)$. In particular, a smaller discrepancy can be seen between $C_{\chi,\text{dec}}^{\text{FD}}$ and $C_{\chi,\text{dec}}^{\text{R}}$, since the latter is also derived from the full Fermi-Dirac statistics.

Since the ratios shown in the right panel of Fig. 4 are predicted via a common thermal parameter κ , the forbidden fermion decay rate can then be simply obtained from the tree-level amplitude with the approximate dispersion relation $\omega^2 - k^2 \approx m_\psi^2(T)$ and rescaling the latter by a constant read from the figure. It enables us to obtain a rather precise forbidden fermion decay rate within the simple tree-level approach by κ -dependent constant rescaling. The results shown in this section not only confirm that using $\omega^2 - k^2 \approx m_\psi^2(T)$ in the tree-level amplitude for forbidden decay is a good approximation [50, 61], but also provide quantitative differences characterized only by the thermal parameter.

4 Scattering

4.1 Double counting and resonant enhancement

The scattering rate directly calculated from Fig. 2 is much more involved. The imaginary parts $\text{Im}\Delta_\pm$ appear both in the numerator and denominator of the off-shell spectral density $\rho_{\psi,\text{off}}$, making the final three-dimensional integration ($dpdk_0dk$) difficult even with a numerical approach. For most situations, the thermal corrections to the scattering processes are significant only when there are IR singularities or resonance. For example, the IR singularity is known in neutrino and electron chirality-flipping processes at finite temperatures [56, 62–64], and the resonant effect from thermal corrections is also known in neutrino oscillations at finite temperature and density [65, 66].

In dealing with the IR singularity or resonance, we can also use a more convenient approach in which the cross section is calculated from a tree-level diagram with a resummed mediator propagator [51, 67, 68]. When applying the effective approach, however, we should take care of the double-counting issue. There are in general two methods to remove the double counting. When the full thermal width of the mediator propagator is unknown, it is convenient to subtract the on-shell point directly from the cross section, and then calculate the forbidden decay rate separately. On the other hand, if the thermal width is known in a given model, a modified Breit-Wigner approximation can be applied to do the subtraction [69, 70], where the decay is automatically included in the cross section.

Nevertheless, the double-counting issue depends on the existence of the resonance, which requires a careful inspection under the perturbative HTL resummation. In the following, let us concentrate on the s -channel double counting and on the hard particle scattering with incoming momenta $p_{\text{hard}} \sim \mathcal{O}(T)$. Generically, hard scattering suffices to be responsible for the nonthermal DM production from thermal particles, since the thermally averaged collision rate $\langle\sigma v\rangle n$ is proportional to the particle-number densities of incoming thermal particles, which are expected to be dominated in the hard-momentum regime:

$$n_{\text{soft}} \propto \int_0^{p_{\text{soft}}} d^3p f^{\text{eq}}(p) \sim p_{\text{soft}}^3, \quad n_{\text{hard}} \propto \int_{p_{\text{soft}}}^{\infty} d^3p f^{\text{eq}}(p) \sim T^3 \gg p_{\text{soft}}^3, \quad (4.1)$$

with $p_{\text{soft}} \sim \mathcal{O}(y_\psi T)$.

At leading order, the mediator is resummed while the external particles are treated effectively massless. At this order, it is usually expected to have an s -channel resonance when the momentum transfer is near the scale of the effective mediator mass. However, when we go beyond the leading order, the external particles are resummed, which also carry effective masses from the plasma. If the thermal masses from the external particles are larger than from the mediator, the resonance expected at leading order would be erased. This is interpreted as the fact that the inverse decay $X + Y \rightarrow Z$ is always kinematically forbidden at all temperatures. This is particularly the case when the mediator is a fermion and the incoming particles contain a scalar boson. For instance, the resummed scalar φ has a thermal correction parameter $\kappa = y_\psi/\sqrt{12}$ [41] from the ψ - η loop, which is larger than the value given in Eq. (3.19).

The above conclusion differs from two fermion scattering mediated by a thermal scalar. As seen from Fig. 3, there is a nearly massless state for a resummed fermion so that the initial fermions can have an approximate dispersion relation $\omega_i^2 - k^2 \approx 0$ while the resummed scalar mediator carries a large thermal mass. When the momentum transfer is at the order of the scalar thermal mass, there is in principle an on-shell crossing and including the resummed scalar mediator in the fermion-pair scattering can enhance the scattering rate by a factor of $\mathcal{O}(1)$ [41].

Since in current scenario the initial particles contain a fermion and a scalar boson, it is not necessary to use the resummed fermion mediator and the scattering rate from a vacuum computation suffices to describe the DM production to a good approximation.

4.2 Tree-level scattering amplitude without thermal correction

The general $2 \rightarrow 2$ scattering rate for the DM production is given by

$$C_{12 \rightarrow \chi\phi} = \int \frac{d^3p_1}{(2\pi)^3 2E_1} \frac{d^3p_2}{(2\pi)^3 2E_2} \frac{d^3p_\chi}{(2\pi)^3 2E_\chi} \frac{d^3p_\phi}{(2\pi)^3 2E_\phi} f_1 f_2 |\mathcal{M}|_{12 \rightarrow \chi\phi}^2 (2\pi)^4 \delta^4, \quad (4.2)$$

where $\delta^4 \equiv \delta^4(P_1 + P_2 - P_\chi - P_\phi)$ and $|\mathcal{M}|_{12 \rightarrow \chi\phi}^2$ is the squared amplitude with spin sum but without spin average. The Pauli blocking and Bose enhancement from the nonthermal DM sector are neglected.

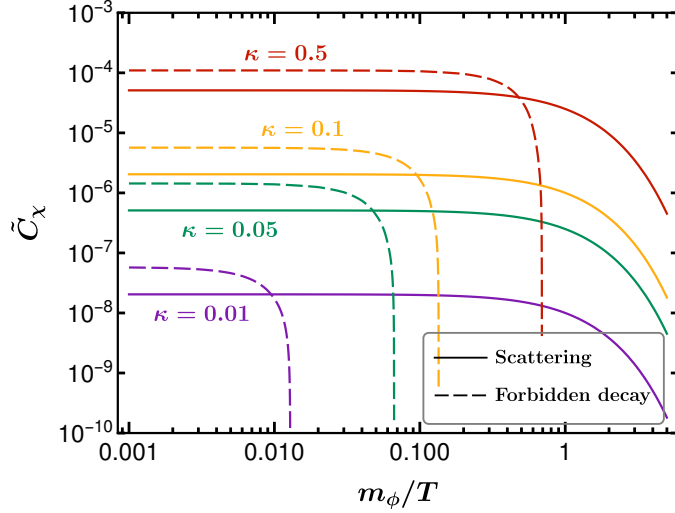


Figure 5. A comparison between the forbidden decay and scattering rates for different thermal parameter κ . Here $\tilde{C}_\chi \equiv y_\chi^{-2} T^{-4} C_\chi$.

For Yukawa interaction, the scattering is $\eta + \varphi \rightarrow \chi + \phi$. The squared amplitude is given by

$$\sum_s |\mathcal{M}|_{\varphi\eta \rightarrow \chi\phi}^2 \approx \frac{y_\chi^2 y_\psi^2}{2} \left(1 - \frac{m_\phi^2}{s}\right) (1 + \cos \theta), \quad (4.3)$$

where we have only kept the highest mass scale from m_ϕ and θ is the angle between the spatial momenta of the incoming and outgoing particles in the center-of-mass frame. Following the conventional phase-space reduction [71], we obtain the collision rate

$$C_{\varphi\eta \rightarrow \chi\phi} = \frac{T}{32\pi^4} \int_{m_\phi^2}^{\infty} ds \sigma_{\varphi\eta \rightarrow \chi\phi} s^{3/2} K_1(\sqrt{s}/T), \quad (4.4)$$

where the cross section without spin average is given by

$$\sigma_{\varphi\eta \rightarrow \chi\phi} = \frac{y_\chi^2 y_\psi^2}{32\pi s} \left(1 - \frac{m_\phi^2}{s}\right)^2. \quad (4.5)$$

In the high-temperature limit $T \gg m_\phi$, the collision rate reduces to

$$C_{\varphi\eta \rightarrow \chi\phi} \approx \frac{y_\chi^2 y_\psi^2}{256\pi^5} T^4. \quad (4.6)$$

In Fig. 5, we show the rates from the forbidden decay and scattering channels. In general, $C_{\chi,\text{dec}}$ is larger than $C_{\chi,\text{scat}}$ when $T > T_c$. Nevertheless, the duration of the forbidden decay is determined by the critical temperature T_c , while the scattering $\eta + \varphi \rightarrow \chi + \phi$ is sufficiently closed only after the freeze-in temperature $T \sim m_\phi > T_c$. It makes the scattering contribution to the final DM relic density generically larger than the forbidden

decay, as we shall discuss below.

5 DM relic density

There are in principle two possibilities for DM relic density. If the scalar ϕ is unstable, it can decay to χ at late times after the dark sector freezes in. Consider first the situation where ϕ has been depleted away. χ is the DM candidate and the relic density is given by

$$\Omega_{\text{DM}}h^2 = \frac{(Y_\chi^{\text{I}} + Y_\chi^{\text{II}})s_0m_\chi}{\rho_c/h^2}. \quad (5.1)$$

where $Y_\chi^{\text{I}} \equiv n_\chi^{\text{I}}/s_{\text{SM}}$ is the yield produced by forbidden decay and scattering while Y_χ^{II} is the yield produced by scalar decay $\phi \rightarrow \psi + \chi$ at late times. $s_{\text{SM}} = 2\pi^2g_sT^3/45$ is the SM entropy density with g_s the effective number of relativistic degrees of freedom. The current value of entropy density is given by $s_0 = 2891.2 \text{ cm}^{-3}$ and the current critical energy density ρ_c is given by $\rho_c = 1.05 \times 10^{-5} h^2 \cdot \text{GeV} \cdot \text{cm}^{-3}$ [72].

The Boltzmann equation for Y_χ^{I} is given by

$$Y_\chi^{\text{I}} = \int_{T_c}^{\infty} \frac{2C_{\chi,\text{dec}}}{s_{\text{SM}}HT} dT + \int_0^{\infty} \frac{2C_{\chi,\text{scat}}}{s_{\text{SM}}HT} dT, \quad (5.2)$$

where the factor of 2 accounts for the CP -conjugated production so that Y_χ is the sum of $\chi + \bar{\chi}$. The forbidden decay ends at $T = T_c$ while the scattering basically ends at $T = \mathcal{O}(m_\phi)$ as the freeze-in temperature is determined by the highest scale in the dark sector. In the second term of Eq. (5.2), we use $T = 0$ as the lower integration limit, which does not cause significant difference after T drops below $m_\phi/5$. Since both $\chi + \bar{\chi}$ and ϕ are produced with the same amount from the forbidden decay and scattering, we have $Y_\chi^{\text{I}} = Y_\phi^{\text{I}}$. Further given that the amount of $\chi + \bar{\chi}$ in late-time production is inherited from Y_ϕ^{I} , we have $Y_\chi^{\text{II}} = Y_\phi^{\text{I}}$.

Consider the second possibility where ϕ is sufficiently long-lived so that it has a lifetime comparable with or longer than the age of the observed universe. The DM relic density in this case consists of ϕ and χ , which is given by

$$\Omega_{\text{DM}}h^2 = \frac{s_0}{\rho_c/h^2}(Y_\chi^{\text{I}}m_\chi + Y_\phi^{\text{I}}m_\phi). \quad (5.3)$$

To see the relative effect of the forbidden decay and the scattering channel, we estimate the ratio $Y_{\chi,\text{scat}}/Y_{\chi,\text{dec}}$, which reads:

$$\frac{Y_{\chi,\text{scat}}}{Y_{\chi,\text{dec}}} \approx \frac{\int_0^{x_{\phi,\text{fi}}} \tilde{C}_{\chi,\text{scat}} dx_\phi}{\int_0^{\sqrt{2}\kappa} \tilde{C}_{\chi,\text{dec}} dx_\phi}, \quad (5.4)$$

where $x_\phi \equiv m_\phi/T$ with $x_{\phi,\text{fi}}$ corresponding to the freeze-in temperature. The evolution of $\tilde{C}_{\chi,\text{dec}}$ and $\tilde{C}_{\chi,\text{scat}}$ can be seen in Fig. 5. Simply taking $\tilde{C}_{\chi,\text{dec}}$ and $\tilde{C}_{\chi,\text{scat}}$ as constants, we obtain $Y_{\chi,\text{scat}}/Y_{\chi,\text{dec}} \propto 1/\kappa$. It points out that the DM relic density from the forbidden decay basically carries an additional power of κ higher than from the scattering channel,

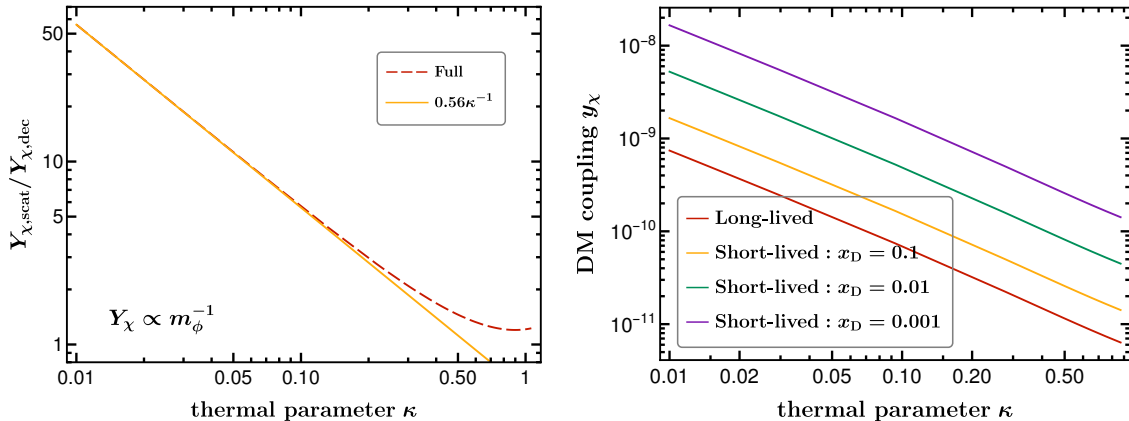


Figure 6. Left: A comparison of DM relic densities from the forbidden decay and scattering channels. Right: The correlation between the DM coupling y_{χ} and the thermal parameter κ for the observed DM relic density. Here $x_D \equiv m_{\chi}/m_{\phi}$.

even though both the decay and scattering rates share the same order of κ (see Eqs. (3.31) and (4.4)), as also found in Refs. [39, 41] in the case of forbidden scalar decay.

The behavior of Eq. (5.4) is shown in the left panel of Fig. 6 as a function of the thermal parameter κ . Note that only the highest scale m_{ϕ} is kept in the yield so that both $Y_{\chi,\text{dec}}$ and $Y_{\chi,\text{scat}}$ are proportional to the inverse scalar mass, as expected from the IR freeze-in mechanism. We can see from the left panel of Fig. 6 that for the fermion mediator the forbidden decay can only be neglected for a very small κ . For a large κ , the contributions from the forbidden decay and the scattering could be comparable. For instance, about 41% of the DM relic density from Eq. (5.1) comes from the forbidden decay if $\kappa = 0.5$, while about 8% of the DM relic density is obtained from the forbidden decay if $\kappa = 0.05$. As already mentioned in Sec. 3.2, we have taken a conservative limit for a Yukawa coupling $y_{\psi} < 1$, and the upper limit of κ depends on the gauge degeneracy of thermal particles η, φ and on possible flavored Yukawa couplings. These effects could further enhance the decay contribution, which is the subject of Sec. 6.

An interesting feature from such a comparison is that we can estimate the effect of the forbidden decay by rescaling the scattering rate, since the ratio given in Eq. (5.4) basically depends on the thermal coupling κ , or the interaction coupling y_{ψ} . Once the thermal interaction of the fermion mediator is known, we can calculate the scattering rate and simply rescale it by a κ - or y_{ψ} -dependent factor to obtain the forbidden decay. As shown in the left panel of Fig. 6, when $\kappa \lesssim 0.2$, the ratio is approximately given by $0.56/\kappa$ and the total DM relic density given in Eq. (5.1) can then be estimated by

$$\Omega_{\text{DM}} h^2 \approx 2 \frac{s_0 m_{\chi}}{\rho_c / h^2} (1 + 1.79\kappa) Y_{\chi,\text{scat}}, \quad (5.5)$$

where $Y_{\chi,\text{scat}}$ comes from the second term in Eq. (5.2).

In the right panel of Fig. 6, we plot the correlation between the DM coupling y_{χ} and the thermal parameter κ by fitting the observed DM relic density $\Omega_{\text{DM}} h^2 = 0.12$ [25].

The long-lived line corresponds to the second possibility from Eq. (5.3), where we have neglected the contribution from the light χ . In this approximation, the DM relic density is independent of m_ϕ since $Y_\phi^1 \propto m_\phi^{-1}$. However, the DM relic density from Eq. (5.3) requires that the scalar should have a lifetime longer than the age of the universe, which is translated into an upper limit of the DM coupling $y_\chi \lesssim 10^{-20}(m_\phi/\text{GeV})^{-1/2}$. Therefore, we can conclude from the right panel of Fig. 6 that for a dark scalar heavier than 1 GeV, the DM relic density results from the lighter fermion χ . For instance, with $y_\chi \simeq 10^{-11}$ and $m_\phi \simeq 10$ GeV, the scalar lifetime is around $\tau_\phi \simeq 0.03$ s. Thus the unstable heavy scalar has decayed away well before the big bang nucleosynthesis epoch.

For the short-lived case from Eq. (5.1), the DM relic density depends on y_χ, κ and the mass ratio in the dark sector $x_D \equiv m_\chi/m_\phi$. We show in the right panel of Fig. 6 for three representative values $x_D = 0.1, 0.01, 0.001$. We can see that when the mass ratio x_D and the thermal parameter κ decrease, a larger DM coupling y_χ is required to match the relic density. However, a large DM coupling could make the dark sector thermalized. To check this, recall that the nonthermal condition, which requires that the thermally averaged scattering rate should be smaller than the Hubble parameter at the freeze-in temperature, is given by

$$\frac{C_{\chi,\text{scat}}}{n_\chi^{\text{eq}}} < H, \quad (5.6)$$

where $n_\chi^{\text{eq}} \approx 0.09T^3$ denotes the thermal particle-number density of χ . The above condition can be translated into an upper limit of the DM coupling $y_\chi \lesssim \mathcal{O}(10^{-4})$. Therefore, for the thermal parameter κ and the mass ratio x_D shown in the right panel of Fig. 6, the dark sector is indeed far from thermal equilibrium.

When κ is much smaller but still able to keep the fermion mediator in thermal equilibrium, the scattering channel for the DM production can also come from the mediator scattering/annihilation, e.g., $\psi + \bar{\psi} \rightarrow \chi + \bar{\chi}$ mediated by the scalar ϕ and $\psi + \bar{\psi} \rightarrow \phi + \phi$ mediated by χ , both of which are not included in previous calculations since we are concerned with a relatively large κ . These scattering channels have rates at $\mathcal{O}(y_\chi^4)$ and could be comparable with the thermal particle scattering $\sim \mathcal{O}(y_\chi^2 y_\psi^2)$ if $y_\chi \sim y_\psi$. For example, when the fermion mediator ψ is a GeV-scale right-handed neutrino in the type-I seesaw framework, the scattering $\psi + \bar{\psi} \rightarrow \chi + \bar{\chi}$ that can generate the observed DM relic density predicts a nonthermal DM coupling $y_\chi \sim \mathcal{O}(10^{-6})$ while the coupling for a GeV-scale right-handed neutrino to keep in thermal equilibrium via neutrino oscillation is required to be $y_\psi > \mathcal{O}(10^{-8})$ [22, 73]. Therefore, for a much smaller thermal parameter κ , the DM production from the mediator scattering/annihilation could be significant. A large thermal parameter κ , on the other hand, is usually more favorable as the strong connection between the SM and the fermion mediator enables us to have more opportunities of DM detection via the very fermion messenger, and is widely predicted in specific scenarios that can explain experimental anomalies, as to be discussed in the following.

6 Application to different thermal Yukawa interactions

We have considered a typical example in Sec. 2 where both the DM-mediator and SM-mediator connections are realized by Yukawa portal interaction. In this section, we shall discuss some specific models to which previous calculations can be applied. The aim of this section is to calculate the DM relic density, following previous sections which combine the forbidden fermion decay and the associated scattering in terms of the thermal parameter κ . We specify some typical thermal interactions with different gauge representations for the thermal particles, and discuss the significance of forbidden fermion decay that could be readily overlooked in the scenarios of light fermion mediators.

It should be mentioned that the observational signatures of these specific scenarios depend not only on the thermal coupling, but also on the masses of thermal particles and the mediator. However, the analyses presented in previous sections only assume that the relevant thermal species are lighter than the heaviest scale in the dark sector. Given that the scale of the dark sector is not known a priori, there is no definite mass limit that can be inferred from the interplay between the mediator and the DM. On the other hand, we can infer from the right panel of Fig. 6 that increasing the thermal coupling κ and the mass hierarchy x_D in the dark sector can open up the DM parameter space towards smaller values, which could help to evade severe observational constraints whenever the detection of DM via the light fermion mediator is concerned. In doing so, i.e., increasing the thermal parameter, the forbidden decay cannot be overlooked. In the following analysis, we commonly assume that there is only one fermion mediator that connects the dark sector to the SM thermal plasma.

6.1 Right-handed fermion mediator

Presumably, the most known example is the Majorana neutrino portal DM [12–22], but ψ_R can also be identified as the right-handed Dirac counterpart of the SM left-handed neutrinos. Both the Majorana and Dirac neutrino mediators allow a dark sector to be produced via the freeze-in mechanism, as long as ψ_R does not have strong gauge interactions. A noticeable difference between the Majorana and Dirac portals is that the latter naturally predicts a very light fermion mediator with mass readily well below the dark scale.

For right-handed neutrino mediators, the left-handed fermion in (2.2) is identified as the SM lepton doublet, while the scalar can either be the SM Higgs doublet or a new Higgs doublet. In the former case, a light right-handed Majorana neutrino with small Yukawa couplings can already be in thermal equilibrium via fast neutrino oscillation [22, 73]. So if the active-sterile neutrino mixing is small, the thermal corrections to the Majorana neutrino would be suppressed. Consequently, the duration of the forbidden decay channel would be quite short and the scattering becomes the dominant channel to generate the DM relic density. Certainly, large Yukawa couplings are still allowed for Majorana neutrinos, in particular, if they couple to a new Higgs doublet. In this latter case, an $\mathcal{O}(1)$ Yukawa coupling between the right-handed neutrino and the new Higgs doublet was interesting, as considered in Dirac neutrino mass origin [74–76] and in explanations of flavor anomalies observed at low-energy experiments [77–80].

With large Yukawa interactions, the forbidden right-handed neutrino decay cannot be neglected. Applying the calculation in Sec. 3, we can readily obtain the thermal mass for the right-handed neutrino,

$$m_\psi^2(T) = \frac{y_\psi^2}{8} T^2, \quad (6.1)$$

and hence $\kappa = y_\psi/\sqrt{8}$. Note that the different thermal mass in Eq. (6.1) does not modify the ratio $Y_{\chi,\text{scat}}/Y_{\chi,\text{dec}}$ in terms of a free κ . To see this, recall that the calculation of forbidden decay is given in terms of $m_\psi \equiv \kappa T$. From Eq. (3.19) to Eq. (6.1), we have $m_\psi \equiv \kappa T \rightarrow \tilde{\kappa} T$, with $\tilde{\kappa} = \sqrt{2}\kappa$. On the other hand, the scattering cross section is now enhanced by a factor of 2 due to the gauge degeneracy, so the yield from Eq. (3.19) to Eq. (6.1) is changed as $Y_{\chi,\text{scat}} \propto y_\psi^2 = (4\kappa)^2 \rightarrow 2y_\psi^2 = (4\tilde{\kappa})^2$. Therefore, for a thermal mass different from Eq. (3.19), the updated ratio $Y_{\chi,\text{scat}}/Y_{\chi,\text{dec}}$ can still be given by a free κ but with an enhanced maximum. For example, the thermal coupling in Eq. (3.19) indicates $0.025 < \kappa < 0.25$ under the condition (3.22), and it is enhanced to be $0.035 < \kappa < 0.35$ in Eq. (6.1).

From the left panel of Fig. 6, we can now obtain the portion from the forbidden decay channel to the DM relic density in the following range:

$$f_{\text{decay}} \equiv \frac{\Omega_{\text{decay}}}{\Omega_{\text{tot}}} \simeq 6\% - 35\%. \quad (6.2)$$

It should be emphasized that we have not taken into account the flavor effects from (2.2). With a single right-handed neutrino mediator, there are in general three coupling constants in (2.2), corresponding to the interactions with three lepton flavors. It is possible that all the three couplings are comparably large. In this case, $y_\psi^2 = y_{\psi,1}^2 + y_{\psi,2}^2 + y_{\psi,3}^2$ can further enhance the thermal mass effect within the condition $0.1 < y_{\psi,i} < 1$. The fraction given in Eq. (6.2) can then reach a maximal value $f_{\text{decay}}^{\text{max}} = 43\%$.

A right-handed fermion mediator can also couple to quark doublets. This can be realized by introducing leptoquarks, which were considered as promising candidates to explain flavor anomalies [81–83]⁴. With a scalar leptoquark, the Yukawa interaction is given by

$$y_{\psi,i} \bar{Q}_{i,L} \psi_R \varphi + \text{h.c.}, \quad (6.3)$$

where $Q_L = (u_L, d_L)^T$ is the quark doublet and the leptoquark scalar doublet φ carries a hypercharge $Y = 1/6$. In this case, the thermal mass of ψ is given by

$$m_\psi^2(T) = \sum_{i=1}^3 \frac{3y_{\psi,i}^2}{8} T^2, \quad (6.4)$$

where the factor of 3 accounts for the color degrees of freedom. If only one coupling is significant, the condition $0.1 < y_{\psi,i} < 1$ would be translated into $0.061 < \kappa < 0.61$. If three

⁴Note that, in such leptoquark scenarios, the Yukawa couplings are generically predicted at $\mathcal{O}(1)$.

Thermalization patterns	Range of $f_{\text{decay,1f}}$ (%)	Range of $f_{\text{decay,3f}}$ (%)
$\bar{L}_i \varphi \psi_R$	[6,35]	[10,43]
$\bar{Q}_i \varphi \psi_R$	[10,43]	[16,45]
$\bar{\psi}_L \varphi \ell_{i,R}$	[4,29]	[7,39]
$\bar{\psi}_L \varphi d_{i,R}$	[7,39]	[12,45]

Table 1. Different thermalization interactions for a right- or left-handed fermion mediator ψ with a Yukawa coupling in the regime: $[0.1, 1]$. 1f assumes that the interaction is dominated by a SM fermion flavor while 3f considers comparable interactions among the three flavors.

couplings are comparably large $y_{\psi,1} \approx y_{\psi,2} \approx y_{\psi,3}$, the range of κ is given by $0.11 < \kappa < 1.1$. In this case, the fraction f_{decay} is estimated to be

$$f_{\text{decay,1f}} = 10\% - 43\%, \quad (6.5)$$

with a one-flavor (1f) dominated coupling and

$$f_{\text{decay,3f}} = 16\% - 45\%, \quad (6.6)$$

with three-flavor (3f) comparable couplings.

6.2 Left-handed fermion mediator

A left-handed fermion mediator can couple to the right-handed DM χ_R via chiral Yukawa interaction. For a nonthermal dark sector via the Yukawa interaction $\bar{\psi}_L \chi_R \phi$, the left-handed mediator cannot have strong gauge interaction. There are some possibilities. For instance, ψ_L can couple to the SM charged-lepton singlet ℓ_R via [84]

$$y_{\psi,i} \bar{\psi}_L \ell_{i,R} \varphi + \text{h.c.}, \quad (6.7)$$

where $y_{\psi,i}$ in general have three couplings to the charged-lepton flavors, ψ_L is a neutral lepton and φ is electrically charged. Here ψ is a SM singlet so that the dark sector does not carry SM gauge charges. Since both φ and ℓ_R are SM gauge singlets, the thermal mass of ψ_L would be given by

$$m_{\psi}^2(T) = \sum_{i=1}^3 \frac{y_{\psi,i}^2}{16} T^2, \quad (6.8)$$

leading to

$$f_{\text{decay,1f}} = 4\% - 29\%, \quad f_{\text{decay,3f}} = 7\% - 39\%, \quad (6.9)$$

for 1f and 3f dominated couplings, respectively.

A left-handed fermion mediator singlet can also couple to right-handed quarks. For

instance, the down-quark singlet d_R couples to ψ_L with a leptoquark scalar φ [85–89]:

$$y_{\psi,i} \bar{d}_{i,R} \psi_L \varphi + \text{h.c.}, \quad (6.10)$$

where the scalar φ is now an $SU(3)_c$ triplet and $SU(2)_L$ singlet, carrying the hypercharge $Y = -1/3$ so that ψ is a SM singlet. The thermal mass in this case is given by

$$m_\psi^2(T) = \sum_{i=1}^3 \frac{3y_{\psi,i}^2}{16} T^2, \quad (6.11)$$

where the factor of 3 accounts for the color degrees of freedom. It then leads to

$$f_{\text{decay,1f}} = 7\% - 39\%, \quad f_{\text{decay,3f}} = 12\% - 45\%. \quad (6.12)$$

The thermalization interactions and the portion of forbidden decay are summarized in Tab. 1. A general expectation is that, for a Yukawa coupling at 0.1–1, the contribution from the forbidden decay can range from 4% to 45%. The largest contribution comes from (6.3) with comparably large Yukawa couplings, where the thermal loop correction to the fermion mediator is enhanced by the gauge degeneracy and the color degrees of freedom.

There is no doubt that a phenomenological study of each pattern deserves comprehensive analyses, especially given that they can arise from crossed areas, ranging from neutrino physics, flavor anomalies to DM physics. The results obtained in this section serve to underlie the detailed investigations when a heavy dark sector is generated by a light fermion mediator.

7 Conclusions

In this work we have concentrated on the freeze-in DM production via a light fermion mediator once thermalized in the early universe. We have used Yukawa portal interactions to capture the basic properties of such a class of DM models, where the scattering and forbidden fermion decay rates carry the same order of coupling constants. The results can be applied to the scenarios of right-handed Majorana/Dirac neutrino portals, as well as the right- and left-handed fermion mediators coupling to the SM fermions, provided that the dark sector is heavier than the mediator and the relevant thermal particles.

The full forbidden decay rate should in general be calculated from the one-loop retarded amplitude at finite temperatures, and is generically overestimated by a tree-level amplitude. Nevertheless, we found that the forbidden decay rate can still be simply obtained from the tree-level amplitude after being rescaled by some constants that depend only on the thermal parameter.

Both the scattering and forbidden fermion decay coexist to generate the DM relic density. The contribution from the forbidden decay is significant when the interaction between the fermion mediator and the thermal plasma is strong. For a Yukawa coupling in the range: 0.1–1, the forbidden decay can contribute to the total DM relic density at the level of 4%–45%, depending on the gauge representations of thermal particles and flavored

Yukawa interactions, and hence cannot be neglected in precise calculation of the DM relic density.

Acknowledgments

The author thanks Xun-Jie Xu for valuable discussions. This work is supported in part by the National Natural Science Foundation of China under grant No. 12141501.

A Thermal one-loop amplitudes

A.1 The DM part

The amplitudes from Fig. 2 are given by

$$\begin{aligned}\Sigma_{+-}^\chi(P) &= -iy_\chi^2 \int \frac{d^4 K}{(2\pi)^4} G_{-+}(K-P) S_{+-}(K) \\ &= \frac{iy_\chi^2}{(2\pi)^2} \int d^4 K \text{sign}(k_0 - p_0) [1 + f_\phi(k_0 - p_0)] f_\psi(k_0) \delta_{K-P} \rho_\psi(K),\end{aligned}\quad (\text{A.1})$$

$$\begin{aligned}\Sigma_{-+}^\chi(P) &= -iy_\chi^2 \int \frac{d^4 K}{(2\pi)^4} G_{+-}(K-P) S_{-+}(K) \\ &= \frac{-iy_\chi^2}{(2\pi)^2} \int d^4 K \text{sign}(k_0 - p_0) f_\phi(k_0) [1 - f_\psi(k_0 - p_0)] \delta_{K-P} \rho_\psi(K),\end{aligned}\quad (\text{A.2})$$

where $\delta_{K-P} \equiv \delta[(K-P)^2 - m_\phi^2]$ and the free scalar propagators G_{-+}, G_{+-} are given by

$$G_{+-}(K) = -2\pi i \text{sign}(k_0) f_\phi(k_0) \delta(K^2 - m_\phi^2), \quad (\text{A.3})$$

$$G_{-+}(K) = -2\pi i \text{sign}(k_0) [1 + f_\phi(k_0)] \delta(K^2 - m_\phi^2), \quad (\text{A.4})$$

while the resummed fermion propagators S_{+-}, S_{-+} are given by Eqs. (3.5) and (3.6).

A.2 The fermion mediator part

The real part of the retarded amplitude $\Sigma_R^\psi(K)$ is equivalent to the time-ordered one $\Sigma_{++}^\psi(K)$, which in the massless limit is given by

$$\begin{aligned}\Sigma_{++}^\psi(K) &= iy_\psi^2 \int \frac{d^4 Q}{(2\pi)^4} G_{++}(Q-K) P_L S_{++}(Q) P_R \\ &= iy_\psi^2 \int \frac{d^4 Q}{(2\pi)^4} \left(\frac{1}{Q^2 + i\epsilon} + 2\pi i f_\eta(|q_0|) \delta(Q^2) \right) P_L Q P_R \\ &\quad \times \left(\frac{1}{(Q-K)^2 + i\epsilon} - 2\pi i f_\varphi(|q_0 - k_0|) \delta[(Q-K)^2] \right),\end{aligned}\quad (\text{A.5})$$

The zero-temperature part is UV divergent, which can be renormalized as usual in zero-temperature QFT. For the finite-temperature part, it reads

$$\begin{aligned}\text{Re}\Sigma_R^\psi(K) &= \frac{y_\psi^2}{(2\pi)^3} \int d^4Q \left(\frac{\delta[(Q-K)^2]}{Q^2} f_\varphi(|q_0 - k_0|) - \frac{\delta(Q^2)}{(Q-K)^2} f_\eta(|q_0|) \right) P_L \not{Q} P_R \\ &= \frac{y_\psi^2}{(2\pi)^3} \int d^4Q \frac{\delta(Q^2)}{(Q-K)^2} \left(f_\varphi(q) P_L(-\not{Q} + \not{K}) P_R - f_\eta(q) P_L \not{Q} P_R \right),\end{aligned}\quad (\text{A.6})$$

where $(Q-K)^2 \neq 0$ and the second equation is obtained by replacing $Q \rightarrow -Q + K$ in the first term of the first equation. The above integration can be done as follows. Integrate q_0 first via $\delta(Q^2)$, then expand the denominator $(Q-K)^2 = K^2 - 2K \cdot Q$ in the HTL approximation: $K^2 \ll q^2$ ⁵, after that integrate the angle $\cos \theta$, and finally integrate the momentum q .

In the HTL approximation, the trace given in Eqs. (3.8) and (3.9) are evaluated to be

$$\begin{aligned}\text{tr}[\not{K} \text{Re}\Sigma_R^\psi(K)] &= \frac{2y_\psi^2}{(2\pi)^2} \int q [f_\varphi(q) + f_\eta(q)] dq + \mathcal{O}(K^2/q^2) \\ &\approx \frac{y_\psi^2}{8} T^2,\end{aligned}\quad (\text{A.7})$$

$$\begin{aligned}\text{tr}[\not{U} \text{Re}\Sigma_R^\psi(K)] &= \frac{y_\psi^2}{(2\pi)^2} \int q [f_\varphi(q) + f_\eta(q)] dq \int d \cos \theta \frac{k_0}{k_0^2 - k^2 \cos^2 \theta} + \mathcal{O}(K^2/q^2) \\ &\approx \frac{y_\psi^2}{16k} \ln \left| \frac{k_0 + k}{k_0 - k} \right| T^2.\end{aligned}\quad (\text{A.8})$$

References

- [1] X. Chu, T. Hambye, and M. H. G. Tytgat, *The Four Basic Ways of Creating Dark Matter Through a Portal*, *JCAP* **05** (2012) 034, [[arXiv:1112.0493](#)].
- [2] T. Hambye, M. H. G. Tytgat, J. Vandecasteele, and L. Vanderheyden, *Dark matter direct detection is testing freeze-in*, *Phys. Rev. D* **98** (2018), no. 7 075017, [[arXiv:1807.05022](#)].
- [3] S. Davidson, S. Hannestad, and G. Raffelt, *Updated bounds on millicharged particles*, *JHEP* **05** (2000) 003, [[hep-ph/0001179](#)].
- [4] J. H. Chang, R. Essig, and S. D. McDermott, *Supernova 1987A Constraints on Sub-GeV Dark Sectors, Millicharged Particles, the QCD Axion, and an Axion-like Particle*, *JHEP* **09** (2018) 051, [[arXiv:1803.00993](#)].
- [5] C. Dvorkin, T. Lin, and K. Schutz, *Making dark matter out of light: freeze-in from plasma effects*, *Phys. Rev. D* **99** (2019), no. 11 115009, [[arXiv:1902.08623](#)]. [Erratum: *Phys.Rev.D* 105, 119901 (2022)].

⁵The forbidden decay primarily stems from a hard ψ propagating near the lightcone. It implies that when using the HTL approximation, the terms from K^2/q^2 have a higher-order y_ψ but k_0/q and k/q are at leading order.

- [6] C. Dvorkin, T. Lin, and K. Schutz, *Cosmology of Sub-MeV Dark Matter Freeze-In*, *Phys. Rev. Lett.* **127** (2021), no. 11 111301, [[arXiv:2011.08186](#)].
- [7] A. Kusenko, *Sterile neutrinos, dark matter, and the pulsar velocities in models with a Higgs singlet*, *Phys. Rev. Lett.* **97** (2006) 241301, [[hep-ph/0609081](#)].
- [8] K. Petraki and A. Kusenko, *Dark-matter sterile neutrinos in models with a gauge singlet in the Higgs sector*, *Phys. Rev. D* **77** (2008) 065014, [[arXiv:0711.4646](#)].
- [9] A. Merle, V. Niro, and D. Schmidt, *New Production Mechanism for keV Sterile Neutrino Dark Matter by Decays of Frozen-In Scalars*, *JCAP* **03** (2014) 028, [[arXiv:1306.3996](#)].
- [10] A. Adulpravitchai and M. A. Schmidt, *A Fresh Look at keV Sterile Neutrino Dark Matter from Frozen-In Scalars*, *JHEP* **01** (2015) 006, [[arXiv:1409.4330](#)].
- [11] M. Drewes and J. U. Kang, *Sterile neutrino Dark Matter production from scalar decay in a thermal bath*, *JHEP* **05** (2016) 051, [[arXiv:1510.05646](#)].
- [12] A. Falkowski, J. Juknevich, and J. Shelton, *Dark matter through the neutrino portal*, [arXiv:0908.1790](#).
- [13] V. González-Macías, J. I. Illana, and J. Wudka, *A realistic model for Dark Matter interactions in the neutrino portal paradigm*, *JHEP* **05** (2016) 171, [[arXiv:1601.05051](#)].
- [14] B. Batell, T. Han, and B. Shams Es Haghi, *Indirect Detection of Neutrino Portal Dark Matter*, *Phys. Rev. D* **97** (2018), no. 9 095020, [[arXiv:1704.08708](#)].
- [15] P. Bandyopadhyay, E. J. Chun, R. Mandal, and F. S. Queiroz, *Scrutinizing Right-Handed Neutrino Portal Dark Matter With Yukawa Effect*, *Phys. Lett. B* **788** (2019) 530–534, [[arXiv:1807.05122](#)].
- [16] M. Becker, *Dark Matter from Freeze-In via the Neutrino Portal*, *Eur. Phys. J. C* **79** (2019), no. 7 611, [[arXiv:1806.08579](#)].
- [17] M. G. Folgado, G. A. Gómez-Vargas, N. Rius, and R. Ruiz De Austri, *Probing the sterile neutrino portal to Dark Matter with γ rays*, *JCAP* **08** (2018) 002, [[arXiv:1803.08934](#)].
- [18] P. Bandyopadhyay, E. J. Chun, and R. Mandal, *Feeble neutrino portal dark matter at neutrino detectors*, *JCAP* **08** (2020) 019, [[arXiv:2005.13933](#)].
- [19] A. Biswas, D. Borah, and D. Nanda, *Light Dirac neutrino portal dark matter with observable ΔN_{eff}* , *JCAP* **10** (2021) 002, [[arXiv:2103.05648](#)].
- [20] R. Coy, A. Gupta, and T. Hambye, *Seesaw neutrino determination of the dark matter relic density*, *Phys. Rev. D* **104** (2021), no. 8 083024, [[arXiv:2104.00042](#)].
- [21] B. Barman, P. S. Bhupal Dev, and A. Ghoshal, *Probing Freeze-in Dark Matter via Heavy Neutrino Portal*, [arXiv:2210.07739](#).
- [22] S.-P. Li and X.-J. Xu, *Dark matter produced from right-handed neutrinos*, [arXiv:2212.09109](#).
- [23] C. A. Argüelles, A. Diaz, A. Kheirandish, A. Olivares-Del-Campo, I. Safa, and A. C. Vincent, *Dark matter annihilation to neutrinos*, *Rev. Mod. Phys.* **93** (2021), no. 3 035007, [[arXiv:1912.09486](#)].
- [24] L. S. Miranda, S. Basegmez du Pree, K. C. Y. Ng, A. Cheek, and C. Arina, *Towards detecting super-GeV dark matter via annihilation to neutrinos*, [arXiv:2211.12235](#).

- [25] **Planck** Collaboration, N. Aghanim et al., *Planck 2018 results. VI. Cosmological parameters*, *Astron. Astrophys.* **641** (2020) A6, [[arXiv:1807.06209](#)]. [Erratum: *Astron.Astrophys.* 652, C4 (2021)].
- [26] J. C. Helo, M. Hirsch, and S. Kovalenko, *Heavy neutrino searches at the LHC with displaced vertices*, *Phys. Rev. D* **89** (2014) 073005, [[arXiv:1312.2900](#)]. [Erratum: *Phys.Rev.D* 93, 099902 (2016)].
- [27] D. Curtin et al., *Long-Lived Particles at the Energy Frontier: The MATHUSLA Physics Case*, *Rept. Prog. Phys.* **82** (2019), no. 11 116201, [[arXiv:1806.07396](#)].
- [28] G. Bélanger et al., *LHC-friendly minimal freeze-in models*, *JHEP* **02** (2019) 186, [[arXiv:1811.05478](#)].
- [29] J. Alimena et al., *Searching for long-lived particles beyond the Standard Model at the Large Hadron Collider*, *J. Phys. G* **47** (2020), no. 9 090501, [[arXiv:1903.04497](#)].
- [30] S. Dodelson and L. M. Widrow, *Sterile-neutrinos as dark matter*, *Phys. Rev. Lett.* **72** (1994) 17–20, [[hep-ph/9303287](#)].
- [31] K. Griest and D. Seckel, *Three exceptions in the calculation of relic abundances*, *Phys. Rev. D* **43** (1991) 3191–3203.
- [32] R. T. D’Agnolo and J. T. Ruderman, *Light Dark Matter from Forbidden Channels*, *Phys. Rev. Lett.* **115** (2015), no. 6 061301, [[arXiv:1505.07107](#)].
- [33] J. McDonald, *Thermally generated gauge singlet scalars as selfinteracting dark matter*, *Phys. Rev. Lett.* **88** (2002) 091304, [[hep-ph/0106249](#)].
- [34] L. J. Hall, K. Jedamzik, J. March-Russell, and S. M. West, *Freeze-In Production of FIMP Dark Matter*, *JHEP* **03** (2010) 080, [[arXiv:0911.1120](#)].
- [35] N. Bernal, M. Heikinheimo, T. Tenkanen, K. Tuominen, and V. Vaskonen, *The Dawn of FIMP Dark Matter: A Review of Models and Constraints*, *Int. J. Mod. Phys. A* **32** (2017), no. 27 1730023, [[arXiv:1706.07442](#)].
- [36] A. Strumia, *Thermal production of axino Dark Matter*, *JHEP* **06** (2010) 036, [[arXiv:1003.5847](#)].
- [37] V. S. Rychkov and A. Strumia, *Thermal production of gravitinos*, *Phys. Rev. D* **75** (2007) 075011, [[hep-ph/0701104](#)].
- [38] J. H. Chang, R. Essig, and A. Reinert, *Light(ly)-coupled Dark Matter in the keV Range: Freeze-In and Constraints*, *JHEP* **03** (2021) 141, [[arXiv:1911.03389](#)].
- [39] L. Darmé, A. Hryczuk, D. Karamitros, and L. Roszkowski, *Forbidden frozen-in dark matter*, *JHEP* **11** (2019) 159, [[arXiv:1908.05685](#)].
- [40] P. Konar, R. Roshan, and S. Show, *Freeze-in dark matter through forbidden channel in $U(1)_{B-L}$* , *JCAP* **03** (2022), no. 03 021, [[arXiv:2110.14411](#)].
- [41] S.-P. Li, *Strong scattering from decay for dark matter freeze-in*, [[arXiv:2211.16802](#)].
- [42] E. Braaten and R. D. Pisarski, *Soft Amplitudes in Hot Gauge Theories: A General Analysis*, *Nucl. Phys. B* **337** (1990) 569–634.
- [43] J. Frenkel and J. C. Taylor, *High Temperature Limit of Thermal QCD*, *Nucl. Phys. B* **334** (1990) 199–216.

- [44] E. Braaten and R. D. Pisarski, *Simple effective Lagrangian for hard thermal loops*, *Phys. Rev. D* **45** (1992), no. 6 R1827.
- [45] M. E. Carrington, D.-f. Hou, and M. H. Thoma, *Equilibrium and nonequilibrium hard thermal loop resummation in the real time formalism*, *Eur. Phys. J. C* **7** (1999) 347–354, [[hep-ph/9708363](#)].
- [46] M. Bellac, *Thermal Field Theory*. Cambridge University Press, 2000.
- [47] H. A. Weldon, *Effective Fermion Masses of Order gT in High Temperature Gauge Theories with Exact Chiral Invariance*, *Phys. Rev. D* **26** (1982) 2789.
- [48] E. Braaten, R. D. Pisarski, and T.-C. Yuan, *Production of Soft Dileptons in the Quark - Gluon Plasma*, *Phys. Rev. Lett.* **64** (1990) 2242.
- [49] A. Peshier and M. H. Thoma, *Quark dispersion relation and dilepton production in the quark gluon plasma*, *Phys. Rev. Lett.* **84** (2000) 841–844, [[hep-ph/9907268](#)].
- [50] C. P. Kiessig, M. Plumacher, and M. H. Thoma, *Decay of a Yukawa fermion at finite temperature and applications to leptogenesis*, *Phys. Rev. D* **82** (2010) 036007, [[arXiv:1003.3016](#)].
- [51] P. B. Arnold, G. D. Moore, and L. G. Yaffe, *Effective kinetic theory for high temperature gauge theories*, *JHEP* **01** (2003) 030, [[hep-ph/0209353](#)].
- [52] D. J. H. Chung, E. W. Kolb, and A. Riotto, *Superheavy dark matter*, *Phys. Rev. D* **59** (1998) 023501, [[hep-ph/9802238](#)].
- [53] D. J. H. Chung, P. Crotty, E. W. Kolb, and A. Riotto, *On the Gravitational Production of Superheavy Dark Matter*, *Phys. Rev. D* **64** (2001) 043503, [[hep-ph/0104100](#)].
- [54] F. Elahi, C. Kolda, and J. Unwin, *UltraViolet Freeze-in*, *JHEP* **03** (2015) 048, [[arXiv:1410.6157](#)].
- [55] H. A. Weldon, *Simple Rules for Discontinuities in Finite Temperature Field Theory*, *Phys. Rev. D* **28** (1983) 2007.
- [56] S.-P. Li and X.-J. Xu, *Neutrino magnetic moments meet precision N_{eff} measurements*, *JHEP* **02** (2023) 085, [[arXiv:2211.04669](#)].
- [57] A. Peshier, K. Schertler, and M. H. Thoma, *One loop selfenergies at finite temperature*, *Annals Phys.* **266** (1998) 162–177, [[hep-ph/9708434](#)].
- [58] C. Kiessig and M. Plumacher, *Hard-Thermal-Loop Corrections in Leptogenesis I: CP-Asymmetries*, *JCAP* **07** (2012) 014, [[arXiv:1111.1231](#)].
- [59] C. Kiessig and M. Plumacher, *Hard-Thermal-Loop Corrections in Leptogenesis II: Solving the Boltzmann Equations*, *JCAP* **09** (2012) 012, [[arXiv:1111.1235](#)].
- [60] M. Drewes and J. U. Kang, *The Kinematics of Cosmic Reheating*, *Nucl. Phys. B* **875** (2013) 315–350, [[arXiv:1305.0267](#)]. [Erratum: *Nucl.Phys.B* 888, 284–286 (2014)].
- [61] G. F. Giudice, A. Notari, M. Raidal, A. Riotto, and A. Strumia, *Towards a complete theory of thermal leptogenesis in the SM and MSSM*, *Nucl. Phys.* **B685** (2004) 89–149, [[hep-ph/0310123](#)].
- [62] P. Elmfors, K. Enqvist, G. Raffelt, and G. Sigl, *Neutrinos with magnetic moment: Depolarization rate in plasma*, *Nucl. Phys. B* **503** (1997) 3–23, [[hep-ph/9703214](#)].

- [63] A. Ayala, J. C. D’Olivo, and M. Torres, *Right-handed neutrino production in dense and hot plasmas*, *Nucl. Phys. B* **564** (2000) 204–222, [[hep-ph/9907398](#)].
- [64] A. Boyarsky, V. Cheianov, O. Ruchayskiy, and O. Sobol, *Evolution of the Primordial Axial Charge across Cosmic Times*, *Phys. Rev. Lett.* **126** (2021), no. 2 021801, [[arXiv:2007.13691](#)].
- [65] L. Wolfenstein, *Neutrino Oscillations in Matter*, *Phys. Rev. D* **17** (1978) 2369–2374.
- [66] D. Notzold and G. Raffelt, *Neutrino Dispersion at Finite Temperature and Density*, *Nucl. Phys. B* **307** (1988) 924–936.
- [67] J.-P. Blaizot and E. Iancu, *A Boltzmann equation for the QCD plasma*, *Nucl. Phys. B* **557** (1999) 183–236, [[hep-ph/9903389](#)].
- [68] J.-P. Blaizot and E. Iancu, *The Quark gluon plasma: Collective dynamics and hard thermal loops*, *Phys. Rept.* **359** (2002) 355–528, [[hep-ph/0101103](#)].
- [69] G. Bélanger, F. Boudjema, A. Goudelis, A. Pukhov, and B. Zaldivar, *micrOMEGAs5.0 : Freeze-in*, *Comput. Phys. Commun.* **231** (2018) 173–186, [[arXiv:1801.03509](#)].
- [70] T. Bringmann, S. Heeba, F. Kahlhoefer, and K. Vangsnes, *Freezing-in a hot bath: resonances, medium effects and phase transitions*, *JHEP* **02** (2022) 110, [[arXiv:2111.14871](#)].
- [71] P. Gondolo and G. Gelmini, *Cosmic abundances of stable particles: Improved analysis*, *Nucl. Phys. B* **360** (1991) 145–179.
- [72] **Particle Data Group** Collaboration, R. L. Workman et al., *Review of Particle Physics*, *PTEP* **2022** (2022) 083C01.
- [73] A. D. Dolgov and F. L. Villante, *BBN bounds on active sterile neutrino mixing*, *Nucl. Phys. B* **679** (2004) 261–298, [[hep-ph/0308083](#)].
- [74] S. Gabriel and S. Nandi, *A New two Higgs doublet model*, *Phys. Lett. B* **655** (2007) 141–147, [[hep-ph/0610253](#)].
- [75] S. M. Davidson and H. E. Logan, *Dirac neutrinos from a second Higgs doublet*, *Phys. Rev. D* **80** (2009) 095008, [[arXiv:0906.3335](#)].
- [76] S.-P. Li, X.-Q. Li, X.-S. Yan, and Y.-D. Yang, *Cosmological imprints of Dirac neutrinos in a keV-vacuum 2HDM**, *Chin. Phys. C* **47** (2023), no. 4 043109, [[arXiv:2202.10250](#)].
- [77] S.-P. Li, X.-Q. Li, Y.-D. Yang, and X. Zhang, *$R_{D^{(*)}}$, $R_{K^{(*)}}$ and neutrino mass in the 2HDM-III with right-handed neutrinos*, *JHEP* **09** (2018) 149, [[arXiv:1807.08530](#)].
- [78] A. Crivellin, D. Müller, and C. Wiegand, *$b \rightarrow s\ell^+\ell^-$ transitions in two-Higgs-doublet models*, *JHEP* **06** (2019) 119, [[arXiv:1903.10440](#)].
- [79] L. Delle Rose, S. Khalil, S. J. D. King, and S. Moretti, *R_K and R_{K^*} in an Aligned 2HDM with Right-Handed Neutrinos*, *Phys. Rev. D* **101** (2020), no. 11 115009, [[arXiv:1903.11146](#)].
- [80] W.-F. Duan, S.-P. Li, X.-Q. Li, and Y.-D. Yang, *Linking anomalies to Hubble tension via a single right-handed neutrino**, *Chin. Phys. C* **47** (2023), no. 3 033102, [[arXiv:2111.05178](#)].
- [81] M. Bauer and M. Neubert, *Minimal Leptoquark Explanation for the $R_{D^{(*)}}$, R_K , and $(g-2)_\mu$ Anomalies*, *Phys. Rev. Lett.* **116** (2016), no. 14 141802, [[arXiv:1511.01900](#)].
- [82] D. Buttazzo, A. Greljo, G. Isidori, and D. Marzocca, *B-physics anomalies: a guide to combined explanations*, *JHEP* **11** (2017) 044, [[arXiv:1706.07808](#)].

- [83] S.-P. Li, X.-Q. Li, X.-S. Yan, and Y.-D. Yang, *Scotogenic Dirac neutrino mass models embedded with leptoquarks: one pathway to address the flavor anomalies and the neutrino masses together*, *Eur. Phys. J. C* **82** (2022), no. 11 1078, [[arXiv:2204.09201](#)].
- [84] Y. Bai and J. Berger, *Lepton Portal Dark Matter*, *JHEP* **08** (2014) 153, [[arXiv:1402.6696](#)].
- [85] M. J. Baker et al., *The Coannihilation Codex*, *JHEP* **12** (2015) 120, [[arXiv:1510.03434](#)].
- [86] R. Mandal, *Fermionic dark matter in leptoquark portal*, *Eur. Phys. J. C* **78** (2018), no. 9 726, [[arXiv:1808.07844](#)].
- [87] M. J. Baker, D. A. Faroughy, and S. Trifinopoulos, *Collider signatures of coannihilating dark matter in light of the B-physics anomalies*, *JHEP* **11** (2021) 084, [[arXiv:2109.08689](#)].
- [88] G. Belanger et al., *Leptoquark manoeuvres in the dark: a simultaneous solution of the dark matter problem and the $R_{D^{(*)}}$ anomalies*, *JHEP* **02** (2022) 042, [[arXiv:2111.08027](#)].
- [89] B. Belfatto, D. Buttazzo, C. Gross, P. Panci, A. Strumia, N. Vignaroli, L. Vittorio, and R. Watanabe, *Dark Matter abundance via thermal decays and leptoquark mediators*, *JHEP* **06** (2022) 084, [[arXiv:2111.14808](#)].